

# Fullerene-Functionalized Gold Nanoparticles: Electrochemical and Spectroscopic Properties

Fengjun Deng,<sup>†</sup> Yiyun Yang,<sup>†</sup> Sungho Hwang,<sup>‡</sup> Young-Seok Shon,<sup>\*,†</sup> and Shaowei Chen<sup>\*,†</sup>

Department of Chemistry and Biochemistry, University of California, Santa Cruz, California 95064, and Department of Chemistry, Western Kentucky University, Bowling Green, Kentucky 42101

**Fullerene (C<sub>60</sub>)-tethered gold nanoparticles were synthesized by the coupling of the fullerene molecules with peripheral amine moieties on the particle surface. The particle composition was determined by thermogravimetric analysis and FT-IR spectroscopy. The resulting particles exhibited unique optical and electrochemical properties. UV–visible measurements showed that the C<sub>60</sub> characteristic absorption remained practically invariant whereas the fluorescence demonstrated rather drastic enhancement of emission efficiency as compared to the behaviors of C<sub>60</sub> monomers. Tethering of C<sub>60</sub> on the particle surface has virtually no effect on the particle molecular capacitance when C<sub>60</sub> is in neutral state, whereas when C<sub>60</sub> is electroreduced, the particle effective capacitance increases drastically, reflected in the quantized capacitance charging measurements. The strong affinity of C<sub>60</sub> to amine moieties was also exploited to assemble multilayers of C<sub>60</sub> and gold particle nanocomposite structures. Quartz crystal microbalance measurements showed quite efficient adsorption of C<sub>60</sub> and particles up to two repeated cycles. However, the voltammetric responses of the surface-confined C<sub>60</sub> and gold particle composite structures were found to be complicated by the inaccessibility of electrolyte counterions due to the compact nature of the surface assemblies.**

Since the discovery of buckminsterfullerene (C<sub>60</sub>) in 1985,<sup>1</sup> fullerenes have been widely studied due to their unique structural, electronic, and spectroscopic properties,<sup>2</sup> which may be exploited for their diverse applications in chemistry, biology, and nanoscience.<sup>3</sup> Of these, recently there has been increasing interest in incorporating C<sub>60</sub> into nanosized particles to fabricate new functional materials, as (transition metals or semiconductor) nanoparticles exhibit size-dependent chemical, electronic, optical, and catalytic characteristics.<sup>4–7</sup> These novel nanocomposite materials<sup>8,9</sup>

may then be utilized for the development of next-generation electronic devices/circuits, such as single-electron transistors, photoelectrochemical conversion devices, etc. For instance, alkanethiolate-protected gold nanoparticles have been synthesized by using the Brust protocol.<sup>10–12</sup> The incorporation of the C<sub>60</sub> moieties into the nanoparticle structure can then be achieved readily by exchange reactions with the mercapto derivatives of C<sub>60</sub> or by surface coupling reactions between C<sub>60</sub> and amine moieties that are located on the periphery of the particle protecting monolayer.<sup>8,9,13</sup> For instance, Kamat et al.<sup>8</sup> synthesized C<sub>60</sub>-functionalized gold nanoparticles and studied the photoantenna effects of the C<sub>60</sub> moieties in photoinduced charge transfer and charge separation.

In this article, by taking advantage of the amination properties of C<sub>60</sub>,<sup>13</sup> we tether various copies of C<sub>60</sub> to gold nanoparticle surfaces by coupling reactions between the C<sub>60</sub> and peripheral amine moieties (from 4-aminothiophenolates, ATP, that are adsorbed onto gold particles). We then study the effects of chemical modifications on C<sub>60</sub> electrochemical and spectroscopic properties. In addition, we examine the influence of C<sub>60</sub> electron-transfer reactions on nanoparticle molecular capacitance. Because of (sub)-attofarad molecular capacitance, nanosized gold particles exhibit quantized charge transfers to the particle double layer, the so-called electrochemical Coulomb staircase charging. These discrete electron-charging behaviors have been found to be sensitive to the particle structures and chemical environments,<sup>11</sup> in particular, the charge state of the peripheral functional moieties that can be manipulated voltammetrically. Thus, in this study we will investigate the effects of C<sub>60</sub> redox reactions on the particle quantized charging.

The strong affinity of C<sub>60</sub> to amine moieties<sup>13</sup> can also be exploited to construct nanocomposite thin films where C<sub>60</sub> and ATP-functionalized gold nanoparticles are assembled by the layer-by-layer adsorption approach. The electrochemistry of both the C<sub>60</sub>

\* To whom all correspondence should be addressed. E-mail: schen@chemistry.ucsc.edu.

<sup>†</sup> University of California.

<sup>‡</sup> Western Kentucky University.

- (1) Kroto, H. W.; Heath, J. R.; O'Brien, S. C.; Curl, R. F.; Smalley, R. E. *Nature* **1985**, *318*, 162.
- (2) Dagani, R. *Chem. Eng. News* **2002**, *80* (24), 32.
- (3) Nakamura, E.; Isobe, H. *Acc. Chem. Res.* **2003**, *36*, 807.
- (4) Schmid, G., Ed. *Clusters and Colloids*; VCH: Weinheim, 1994.
- (5) Hayat, M. A., Ed. *Colloidal Gold: Principles, Methods, and Applications*; Academic Press: San Diego, 1991.
- (6) Alivisatos, A. P. *J. Phys. Chem.* **1996**, *100*, 13326.
- (7) (a) Markovich, G.; Collier, C. P.; Henrichs, S. E.; Remacle, F.; Levine, R. D.; Heath, J. R. *Acc. Chem. Res.* **1999**, *32*, 415. (b) Remacle, F.; Levine, R. D. *ChemPhysChem* **2001**, *2*, 20.

- (8) Sudeep, P. K.; Ipe, B. I.; Thomas, K. G.; George, M. V. Barazzouk, S.; Hotchandani, S.; Kamat, P. V. *Nano Lett.* **2002**, *2*, 29.
- (9) Fujihara, H.; Nakai, H. *Langmuir* **2001**, *17*, 6393.
- (10) Brust, M.; Walker, M.; Bethell, D.; Schiffrin, D. J.; Whyman, R. *J. Chem. Soc., Chem. Commun.* **1994**, 801.
- (11) Templeton, A. C.; Wuelfing, W. P.; Murray, R. W. *Acc. Chem. Res.* **2000**, *33*, 27.
- (12) Whetten, R. L.; Shafiqullin, M. N.; Khoury, J. T.; Schaaff, T. G.; Vezmar, I.; Alvarez, M. M.; Wilkinson, A. *Acc. Chem. Res.* **1999**, *32*, 397.
- (13) (a) Shon, Y.-S.; Choo, H. *Chem. Commun.* **2002**, 2560. (b) Innocenzi, P.; Brusatin, G. *Chem. Mater.* **2001**, *13*, 3126. (c) Mirkin, C. A.; Caldwell, W. B. *Tetrahedron* **1996**, *52*, 5113 and references therein. (d) Choi, S. Y.; Lee, Y.-J.; Park, Y. S.; Ha, K.; Yoon, K. B. *J. Am. Chem. Soc.* **2000**, *122*, 5201.

and nanoparticles is examined and compared to the solution counterparts.

## EXPERIMENTAL SECTION

**Chemicals.** Tetra-*n*-butylammonium perchlorate (TBAP, 99%, Acros) was recrystallized twice prior to use. Bis-2-aminomethyl disulfide dihydrogen chloride (cystamine, 97%, Aldrich), sodium bicarbonate (Fisher), fullerene (99%, Acros), sodium borohydride (98%, Avocado), tetra-*n*-octylammonium bromide (98%, Aldrich), *n*-hexanethiol (96%, Acros), and 4-aminothiophenol (98%, Acros) were used as received. All solvents were purchased from typical commercial sources and also used as received.

**Synthesis of C<sub>60</sub>-Tethered Gold Particles.** The synthesis of C<sub>60</sub>-tethered gold nanoparticles has been described previously.<sup>13a</sup> First, *n*-hexanethiolate-protected gold (AuC<sub>6</sub>) nanoparticles were synthesized using the modified Brust reaction,<sup>10</sup> which then underwent core size fractionation and thermal annealing treatment to reduce the size dispersity.<sup>11,12</sup> The fraction with core diameter of ~2 nm was used for the subsequent studies. Second, the above-obtained AuC<sub>6</sub> particles then mixed with a calculated amount of ATP in dichloromethane for exchange reactions.<sup>11</sup> The resulting particles, ATPAuC<sub>6</sub> (with a molecular composition of ATP<sub>22</sub>Au<sub>314</sub>-C<sub>60</sub> as determined by <sup>1</sup>H NMR spectroscopy), were then used for C<sub>60</sub> functionalization.<sup>13</sup> In a typical reaction, 10 μmol of C<sub>60</sub> and 2.5 μmol of ATPAuC<sub>6</sub> were codissolved in 25 mL of toluene under vigorous stirring for 3 days at room temperature. The solvent (toluene) was removed by rotary evaporation. The crude products were dissolved in CH<sub>2</sub>Cl<sub>2</sub>, and insoluble materials were filtered off. The filtrate was placed under vacuum, and CH<sub>2</sub>Cl<sub>2</sub> was removed. The particles were redissolved in 2 mL of CH<sub>2</sub>Cl<sub>2</sub> and placed in a centrifuge tube into which 2 mL of ethanol was also added. The solution was then centrifuged for 10 min. The precipitate (unbound free C<sub>60</sub>) was removed, and an additional 2 mL of ethanol was added to the CH<sub>2</sub>Cl<sub>2</sub>/EtOH solution. The solution was centrifuged again for 10 min. This process was repeated several times until TLC results (mobile phase, toluene) showed the solution was free of unbound C<sub>60</sub>. The removal of C<sub>60</sub> was indicated by the disappearance of a C<sub>60</sub> band on TLC plates. The resultant C<sub>60</sub>-tethered gold (C<sub>60</sub>-ATPAuC<sub>6</sub>) nanoparticles were found to be soluble in various organic solvents including toluene, dichloromethane, ethanol, and 2-propanol.

**Thermogravimetric Analysis (TGA).** TGA was performed with a TA Instruments TGA2950 using an ultrahigh purity nitrogen atmosphere, with data recorded from room temperature to 600 °C at a heating rate of 20 °C/min. From TGA measurements (Supporting Information), it was estimated that the loading of C<sub>60</sub> was ~6/particle.

**Spectroscopy.** Infrared spectra were obtained, using a Perkin-Elmer 1600 FT-IR spectrometer, of films of MPCs pressed into a KBr plate. The spectra were recorded from 4500 to 450 cm<sup>-1</sup>. Multiple bands near 1600 cm<sup>-1</sup> were observed which indicated the presence of different C=C functional groups in C<sub>60</sub> and 4-aminothiophenolate ligands of C<sub>60</sub>-ATPAuC<sub>6</sub> (Supporting Information). UV-visible experiments were carried out with an ATI Unicam UV4 spectrometer. Photoluminescence properties of C<sub>60</sub>-tethered gold nanoparticles were studied with a PTI fluorospectrometer. Particle solutions were prepared at a concentration of 1 mg/mL in toluene (HPLC grade).

**Layer-by-Layer Assembly of C<sub>60</sub> and C<sub>60</sub>AuATP.** C<sub>60</sub> and ATPAuC<sub>6</sub> were self-assembled onto a gold electrode surface by the layer-by-layer (LbL) approach.<sup>13a</sup> Briefly, a cleaned gold electrode was first immersed into an ethanolic solution of 1 mM cystamine for 24 h. The cystamine-modified electrode was then incubated in a toluene solution containing C<sub>60</sub> (1 mg/mL) for up to 4 days to achieve the first adsorbed layer of C<sub>60</sub>. The resulting electrode was then immersed into a toluene solution of C<sub>60</sub>AuATP (1 mg/mL) for 2 days so that an overlayer of ATPAuC<sub>6</sub> particles was formed. By repeating the deposition cycle into these two solutions (C<sub>60</sub> and ATPAuC<sub>6</sub>), one can in principle build up a multilayer structure of nanoparticles and C<sub>60</sub> molecules. It should be noted that the electrode was rinsed with copious amounts of the respective solvents in each deposition step and dried in a gentle N<sub>2</sub> stream prior to being introduced into the next deposition solution.

**Quartz Crystal Microbalance (QCM) Experiment.** The quartz crystals (International Crystal Manufacturing) were made from polished quartz plates with a resonant frequency of 8 MHz and a crystal diameter of 14 mm. A 10-nm layer of Cr was first deposited onto the center of the quartz crystals (diameter 5 mm) as the adhesion layer, followed by 100 nm of gold. The crystals were subjected to UV-ozone cleaning (UVO Cleaner Model 42, Jelight Co.) for 15 min prior to immersion into the cystamine solution for monolayer coating. The layer assemblies were fabricated by using the above LbL approach where the frequency shift in each deposition step was measured in air.

**Electrochemistry.** Electrochemical measurements were carried out with a CHI 440 electrochemical work station (with the capability of QCM measurements). A gold electrode was used as the working electrode, a Ag/AgCl wire was used as the quasi-reference electrode, and the counter electrode was a Pt coil. The solutions were deaerated for at least 15 min with high-purity nitrogen (Airgas) before data acquisition and blanketed with a nitrogen atmosphere during the entire experiment procedure.

## RESULTS AND DISCUSSION

**Electrochemistry.** Monodisperse gold nanoparticles in solutions exhibit quantized charging to the particle molecular capacitance, reflected in a series of well-defined voltammetric peaks where the potential spacing ( $\Delta V$ ) between neighboring peaks is inversely proportional to the particle capacitance ( $C_{MPC} = e/\Delta V$ , with  $e$  being the electronic charge).<sup>11</sup> As  $C_{MPC}$  can be varied by the particle chemical structure, the resulting voltammetric responses change accordingly. Figure 1 shows the cyclic (CV, A) and differential pulse (DPV, B) voltammograms of C<sub>60</sub>, ATPAuC<sub>6</sub> and C<sub>60</sub>-tethered gold (C<sub>60</sub>-ATPAuC<sub>6</sub>) nanoparticles. It can be seen that there are three pairs of voltammetric waves at -0.55, -1.00, and -1.49 V for the C<sub>60</sub> solution (green curves), with a peak splitting ( $\Delta E_p$ ) less than 90 mV at 100 mV/s indicating quasi-reversible electron-transfer processes. These are attributed to the successive 1e<sup>-</sup> reduction of the C<sub>60</sub> molecules, i.e., C<sub>60</sub><sup>0/-1</sup>, C<sub>60</sub><sup>-1/-2</sup>, and C<sub>60</sub><sup>-2/-3</sup> couples, respectively, as observed previously.<sup>14,15</sup> For the ATPAuC<sub>6</sub> particles, a series of well-defined voltammetric peaks can be found within the wide potential range of -1.8 to +0.6 V

(14) Prato, M.; Maggini, M. *Acc. Chem. Res.* **1998**, *31*, 519.

(15) (a) Xie, Q.; Perez-Cordero, E.; Echegoyen, L. *J. Am. Chem. Soc.* **1992**, *114*, 3978. (b) Ohsawa, Y.; Saji, T.; *J. Chem. Soc., Chem. Commun.* **1992**, 781.

(c) Zhou, F.; Jehoulet, C.; Bard, A. J. *J. Am. Chem. Soc.* **1992**, *114*, 11004.

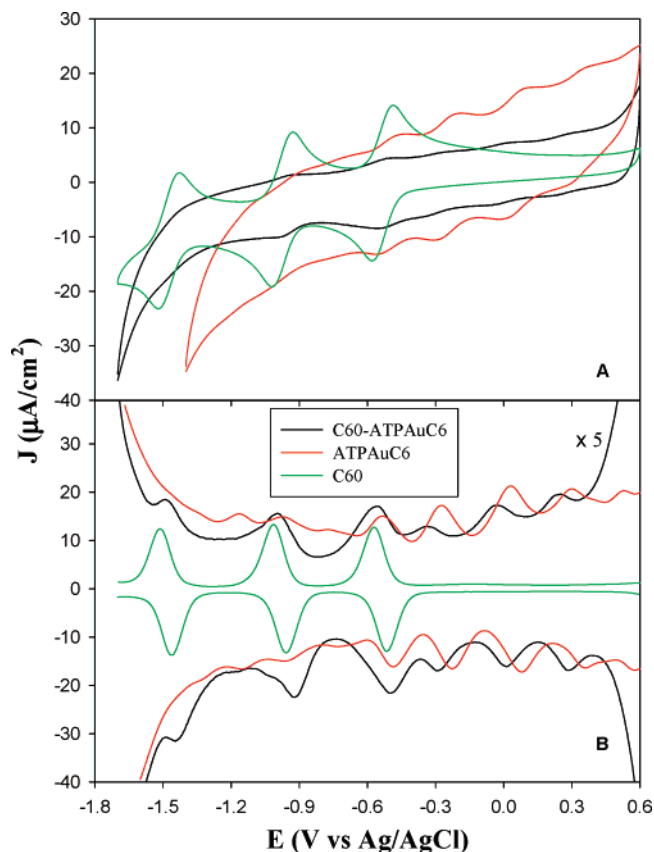


Figure 1. Cyclic (CVs, A) and differential pulse (DPVs, B) voltammograms of  $C_{60}$ , ATPAuC6, and  $C_{60}$ -functionalized ATPAuC6 nanoparticles at a gold electrode (area either 0.64 or 1.56 mm<sup>2</sup>) in a mixed solvent of acetonitrile and toluene (v/v 1:2) containing 0.1 M TBAP. Concentrations:  $C_{60}$ , 1.39 mM; ATPAuC6 particles, 46.8  $\mu$ M;  $C_{60}$ -ATPAuC6 particles, 39  $\mu$ M. In (A), the potential scan rate is 100 mV/s; and in (B), dc potential ramp 20 mV/s, pulse amplitude 50 mV, and pulse width 200 ms.

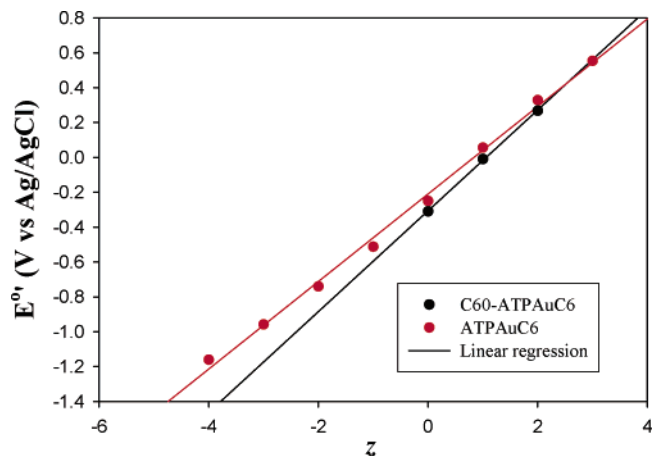


Figure 2. Variation of particle charging peak potentials with particle charge states. Symbols are experimental data and lines are linear regressions.

(red curves). These are ascribed to the quantized charge transfer to the nanoparticle molecular capacitance.<sup>11,16</sup> Figure 2 depicts the variation of the peak (formal) potential ( $E_{z,z-1}^{o'}$ ) with particle charge state ( $z$ ), which shows a linear relationship as expected from<sup>16</sup>

$$E_{z,z-1}^{o'} = E_{PZC} + ((z - (1/2))e/C_{MPC}) \quad (1)$$

where  $E_{PZC}$  is the particle potential of zero charge. From the linear regression (Figure 2), one can then evaluate the particle molecular capacitance,  $C_{MPC} = 0.64$  aF.

When these particles are tethered with several copies of  $C_{60}$  moieties, the voltammetric current is the combined contribution of the particle quantized charging and  $C_{60}$  faradaic reactions (Figure 1, black curves). There are two areas that warrant attention here. First, in the potential range of  $-0.5$  to  $+0.6$  V, there are three pairs of voltammetric peaks ascribed to the particle quantized charging. Again, from the variation of the peak potentials with particle charge state (Figure 2), the particle capacitance can be evaluated as well, which is 0.55 aF. It should be noted that the capacitance evaluated from eq 1 reflects the average within the corresponding potential range. Thus, if one examines the variation of particle peak potential versus charge state within the same potential range, the particle capacitance is essentially invariant. This indicates that, in its neutral state, peripheral  $C_{60}$  moieties do not exhibit significant impact on the particle surface dielectric properties and hence particle capacitance. Second, at potential more negative than  $-0.5$  V, there are also three pairs of voltammetric waves,  $-0.54$ ,  $-1.06$ , and  $-1.46$  V, which correspond very well to those of the  $C_{60}$  molecules (vide ante). This suggests that the electronic interactions between the peripheral  $C_{60}$  moieties and the Au cores should be relatively weak, namely, the  $C_{60}$  energetic states should remain similar to those of free  $C_{60}$  monomers. In addition, interestingly, the peak splitting ( $\Delta E_p$ ) is found to be  $\sim 45$  mV, only half of that with  $C_{60}$  monomers (vide ante). One may also note that, in this negative potential region, the particle quantized charging feature becomes virtually invisible (Figure 1), as compared to that of ATPAuC6 particles. This can be, at least in part, explained by the fact that the peripheral  $C_{60}$  moieties are now (negatively) charged in this potential region, which renders the particle capacitance to increase severalfold and hence diminishing quantized charging features. Similar responses have been observed previously with ferrocene-tethered gold particles,<sup>17</sup> where the particle effective molecular capacitance increases drastically when the peripheral ferrocene moieties are electrooxidized into ferrocenium.

**Spectroscopies.** Figure 3 compares the UV-visible absorption profiles of  $C_{60}$ , AuC6, ATPAuC6, and  $C_{60}$ -tethered gold ( $C_{60}$ -ATPAuC6) nanoparticles. Nanosized gold particles typically exhibit an absorption band at  $\sim 520$  nm, the so-called surface plasmon resonance, which superimposes onto an exponential decay Mie scattering profile.<sup>11,12</sup> It has been found that the intensity and energy of the surface plasmon band depend on the particle size, shape, and local environment. For the particles used in the present study (2-nm diameter), the surface plasmon band is very broad and weak. Using second-order derivatives of the respective absorption spectrum, one can then determine the peak position: AuC6 at 522 nm (blue curve) with ATPAuC6 (green curve) and  $C_{60}$ -ATPAuC6 (red curve) at 536 nm. The observed red-shift upon

(16) Chen, S.; Murray, R. W.; Feldberg, S. W. *J. Phys. Chem. B* **1998**, *102*, 9898.  
 (17) (a) Green, S. J.; Stokes, J. J.; Hostetler, M. J.; Pietron, J. J.; Murray, R. W. *J. Phys. Chem. B* **1997**, *101*, 2663. (b) Green, S. J.; Pietron, J. J.; Stokes, J. J.; Hostetler, M. J.; Vu, H.; Wuelfing, W. P.; Murray, R. W. *Langmuir* **1998**, *14*, 5612.

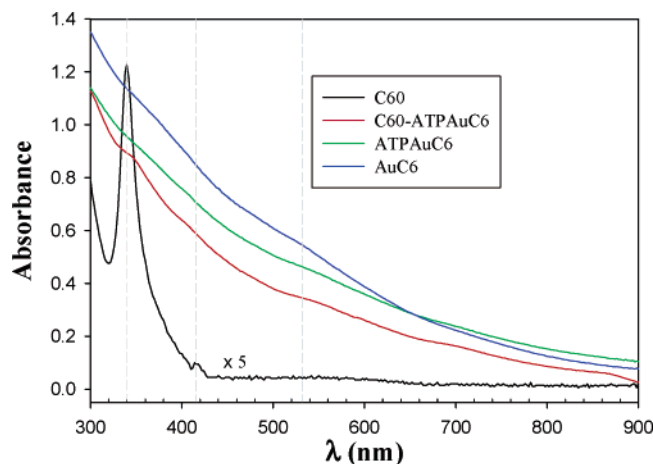


Figure 3. UV-visible absorption spectra of  $C_{60}$ , ATPAuC6 and  $C_{60}$ -functionalized ATPAuC6 nanoparticles. The samples were all dissolved in toluene at the following concentrations:  $C_{60}$ , 6.39  $\mu\text{M}$ ; ATPAuC6, 1.06  $\mu\text{M}$ ;  $C_{60}$ -ATPAuC6, 1.0  $\mu\text{M}$ .

exchange reaction (with ATP) may be attributed to the introduction of more polar ligands into the particle protecting layers, as well as possible enhanced electronic interactions between the aryl  $\pi$ -electrons and core d-electrons (likely due to the electron-donating amino groups). Similar red-shift was also observed with hydroxythiophenol-functionalized gold particles,<sup>18</sup> whereas a blue-shift was found when electron-withdrawing nitrothiophenols<sup>19</sup> were introduced into the gold nanoparticle protecting monolayers.

For  $C_{60}$  monomers (black curve), a characteristic absorption peak can be observed at 340 nm along with a much weaker band at 416 nm. When the  $C_{60}$  moieties are tethered onto gold particle surfaces, the main absorption peak is also found at 340 nm. However, one may note that the intensity is much smaller (the effective concentrations of  $C_{60}$  are very comparable in these two cases), a good indication of amination of  $C_{60}$  molecules.<sup>13</sup> In addition, a small and broad shoulder peak can be found at 408 nm (again, from the second-order derivative of the absorption spectrum) for the  $C_{60}$ -ATPAuC6 particles, which corresponds to the electronic transition at 416 nm observed with pristine  $C_{60}$ . It is likely that the small blue-shift arises from the saturation of one of the double bonds of  $C_{60}$  by the amination reaction.<sup>14</sup>

More interesting spectroscopic responses are observed in fluorescence measurements. Figure 4 shows the fluorescence spectra of  $C_{60}$  monomers, ATPAuC6, and  $C_{60}$ -tethered gold nanoparticles. For  $C_{60}$  monomers (black curves), a broad excitation peak can be found at 357 nm while the corresponding (relatively weak and broad) emission peak, is centered at 440 nm. In contrast, when  $C_{60}$  moieties are tethered onto the gold nanoparticle surface (red curves), the excitation spectrum exhibits several fine features, with peaks at 303, 350, 362, 382, and 406 nm; whereas a major emission peak can be found at 440 nm, which is at the same wavelength position as that of  $C_{60}$  monomers. The appearance of these excitation fine structures might be indicative of the splitting of the originally conjugated energy states due to the amination of the  $C_{60}$  moieties by ATP ligands. Alternatively, they might also be attributable to the contribution of the Au particles, as within the same energy range, ATPAuC6 particles (blue curves) also

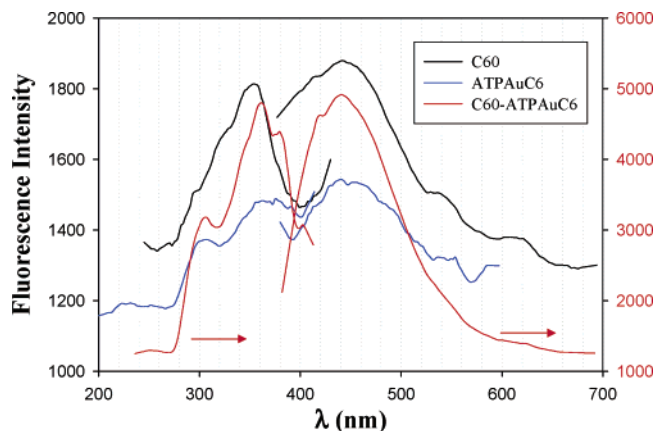


Figure 4. Fluorescence spectra of  $C_{60}$ , ATPAuC6, and  $C_{60}$ -functionalized ATPAuC6 nanoparticles. The excitation and emission spectra were collected under these conditions:  $C_{60}$ ,  $\lambda_{\text{em}} = 450$  nm,  $\lambda_{\text{ex}} = 357$  nm; ATPAuC6,  $\lambda_{\text{em}} = 414$  nm,  $\lambda_{\text{ex}} = 360$  nm;  $C_{60}$ -ATPAuC6,  $\lambda_{\text{em}} = 433$  nm,  $\lambda_{\text{ex}} = 362$  nm. Other experimental conditions the same as those in Figure 3.

show a similar excitation and emission profile. Photoluminescence of alkanethiolate-protected gold particles has been reported previously.<sup>20–22</sup> However, the luminescence is typically observed at much lower energy positions. For instance, near-infrared and red emissions have been reported by the Whetten<sup>20</sup> and Murray<sup>21</sup> groups for particles of similar core sizes. For much smaller particles (e.g.,  $\text{Au}_{11}$  protected by a dodecanethiolate monolayer),<sup>22</sup> the photoluminescence emission was observed at 840 nm, which was ascribed to the electronic transitions involving surface trap states. Photoluminescence of gold nanoparticles in the blue region has only been reported with octagold ( $\text{Au}_8$ ) nanoclusters stabilized in a dendrimer matrix.<sup>23</sup> However, the particles used in the present study are much larger (see the Experimental Section). Thus, it is somewhat surprising that a blue luminescence emission is still observed here. Further studies are desired to understand the origin of this phenomenon.

In addition, one might also note that the luminescence intensity is much greater for  $C_{60}$ -tethered gold particles than that of the  $C_{60}$  monomers or the particles without any  $C_{60}$  moieties (note that the y axes are of different scales). Considering the similar optical absorbance in this wavelength range, one can readily see that the quantum yield of  $C_{60}$ -tethered particles should be greater than that of the pristine  $C_{60}$  monomers or the gold particles. In fact, from Figure 4, the fluorescence quantum yield (QY) of  $C_{60}$ -tethered gold nanoparticles can be estimated to be  $\sim 9.1 \times 10^{-4}$ ,  $\sim 3$ -fold larger than that of the reported value for pristine  $C_{60}$  in toluene ( $3.2 \times 10^{-4}$ ).<sup>24</sup> In comparison, triazolinfullerene<sup>25</sup> showed a QY of  $6.0 \times 10^{-4}$ . At first glance, the observed enhancement of quantum yield is quite surprising, as it had been found previously that the photoluminescence for fluorophores anchored onto metal particle surfaces was easily quenched (absorbed) because of the efficient energy transfer between the fluorophores and the particle

(18) Chen, S. *Langmuir* **1999**, *15*, 7551.

(19) Chen, S.; Huang, K. *Langmuir* **2000**, *16*, 2014.

(20) (a) Bigioni, T. P.; Whetten, R. L.; Dag, Ö. *J. Phys. Chem. B* **2000**, *104*, 6983. (b) Link, S.; Beeby, A.; FitzGerald, S.; El-Sayed, M. A.; Schaaff, T. G.; Whetten, R. L. *J. Phys. Chem. B* **2002**, *106*, 3410.

(21) Huang, T.; Murray, R. W. *J. Phys. Chem. B* **2001**, *105*, 12498.

(22) Yang, Y.; Chen, S. *Nano Lett.* **2003**, *3*, 75.

(23) Zheng, J.; Petty, J. T.; Dickson, R. M. *J. Am. Chem. Soc.* **2003**, *125*, 7780.

(24) Ma, B.; Sun, Y.-P. *J. Chem. Soc., Perkin Trans. 2* **1996**, 2157.

(25) González, S.; Martín, N.; Swartz, A.; Guldi, D. M. *Org. Lett.* **2003**, *5*, 557.

cores.<sup>26</sup> In the present study, both the particle cores and the fluorophores (C<sub>60</sub>) demonstrate photoactivities with similar excitation and emission energies (Figure 4); thus, the collective luminescence emission becomes more effective because of less energy dissipation due to nonradiative energy transfer from the peripheral C<sub>60</sub> moieties to the gold cores.

When the C<sub>60</sub> molecules are functionalized with organic tethers, typically a rather well-defined luminescence emission can be seen in the red.<sup>8,25,27</sup> For instance, the mercapto derivatives of C<sub>60</sub> by a pyrrolidine linkage exhibit an emission at 740 nm.<sup>8</sup> However, when these C<sub>60</sub> moieties are attached to gold nanoparticle surfaces, this low-energy fluorescence is quenched effectively.<sup>8</sup> Consistently, in our present study, we observed no detectable luminescence in this wavelength range with the C<sub>60</sub>-tethered gold nanoparticles. In our previous study,<sup>28</sup> we found that the fluorescence (peaked at 800 nm) of PbS nanoparticles could be readily absorbed by metal nanoparticles (Au, Ag, or Pd), which were codissolved in the solution, despite relatively low absorption of metal nanoparticles in this wavelength range.

**Layer-by-Layer Assembly.** In the following sections, we will focus on the organized assemblies of C<sub>60</sub> and nanoparticles on electrode surfaces. First, we used QCM to monitor the dynamics of the layer-by-layer assembling of C<sub>60</sub> and ATPAuC6 particles. Since the frequency change ( $\Delta f$ ) directly reflects the interfacial mass change ( $\Delta m$ , per unit surface area), according to the Sauerbrey equation<sup>29</sup>

$$\Delta m = -\sqrt{\rho_q \mu_q / 2f_0^2} \Delta f \quad (2)$$

where  $f_0$  is the resonant frequency of the quartz crystal (8 MHz in the present case),  $\rho_q$  is the density of quartz (2.648 g/cm<sup>3</sup>), and  $\mu_q$  is its shear modulus (2.947 × 10<sup>11</sup> dyn/cm<sup>2</sup> for AT-cut quartz). Thus, by measuring the frequency change in each deposition step, one can easily evaluate the corresponding surface coverage. After the formation of a cystamine self-assembled monolayer, the electrode was immersed into a C<sub>60</sub> solution where C<sub>60</sub> molecules were immobilized onto the electrode surface via amination reactions.<sup>13,30,31</sup> The mass increase after 80 h of incubation was measured to be 3.45 × 10<sup>-10</sup> mol/cm<sup>2</sup>. By assuming a close-packed hexagonal molecular arrangement, the full monolayer coverage of C<sub>60</sub> (diameter, 7 Å) is anticipated to be 4.10 × 10<sup>-10</sup> mol/cm<sup>2</sup>. Thus, the first layer of C<sub>60</sub> is ~84.1% of a full monolayer. In the subsequent adsorption of ATPAuC6 particles onto the C<sub>60</sub> layer (72 h), the particle surface coverage was estimated to be 5.44 × 10<sup>-11</sup> mol/cm<sup>2</sup>. This is ~3.4 times the theoretical full monolayer coverage of particles (1.61 × 10<sup>-11</sup> mol/cm<sup>2</sup> by assuming a close-packed, but nonintercalated, hexagonal

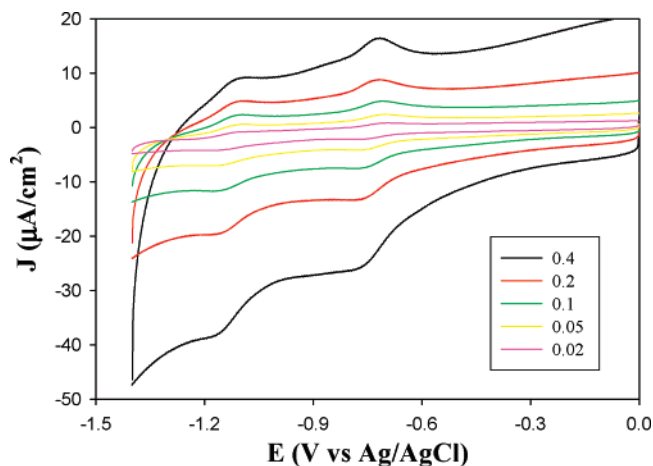


Figure 5. Cyclic voltammograms of C<sub>60</sub> immobilized onto a cystamine self-assembled monolayer on a gold electrode surface in CH<sub>2</sub>-Cl<sub>2</sub> containing 0.1 M TBAP. Electrode area, 0.79 mm<sup>2</sup>. Potential scan rates shown as figure legends in V/s.

arrangement of particles). One possible explanation is the formation of particle multilayers that might arise from the H-bonding interactions through the amine moieties (ATP) as well as ligand intercalation. In the second deposition cycle, the amount of C<sub>60</sub> adsorbed onto the ATPAuC6 particle layer (72 h) was 3.41 × 10<sup>-10</sup> mol/cm<sup>2</sup>, very close to that of the first deposition; whereas the next deposition of ATPAuC6 particles (also after 72 h) was only 1.25 × 10<sup>-11</sup> mol/cm<sup>2</sup>, close to 80% of a full monolayer coverage, substantially smaller than that in the first deposition. Further buildup of more surface layers becomes less effective.

The above study demonstrates that, by taking advantage of C<sub>60</sub> amination, surface nanocomposite layers of gold particles and C<sub>60</sub> can be built up with rather high surface coverage. The corresponding electrochemistry of these layer structures will then be carried out and compared, as detailed below.

**Electrochemistry of Surface-Immobilized Layers.** Figure 5 shows the CV of a C<sub>60</sub> overlayer adsorbed onto a preformed cystamine monolayer on a gold electrode surface in 0.1 M TBAP/CH<sub>2</sub>Cl<sub>2</sub>. Two pairs of voltammetric waves can be seen at -0.77 and -1.17 V, which are ascribed to the first and second one-electron redox reactions of the C<sub>60</sub> molecules. However, as compared to those of C<sub>60</sub> in solution (vide ante, Figure 1), these voltammetric responses show a cathodic shift of 0.27 and 0.17 V, respectively, for the first and second peaks. Nonetheless, the peak splitting ( $\Delta E_p$ ) is ~60 mV, slightly smaller than that with C<sub>60</sub> in solutions (Figure 1). In addition, the peak currents exhibit a linear dependence on potential scan rates, consistent with surface-confined systems (not shown), and from the slope one can estimate the (effective) surface coverage of C<sub>60</sub>, which is ~9.38 × 10<sup>-12</sup> mol/cm<sup>2</sup>. This is only a very small fraction (~3%) of that obtained in the above QCM measurements. Similar weak voltammetric responses have also been observed previously with C<sub>60</sub> adsorbed onto aminopropylsilylated indium-tin-oxide surfaces.<sup>30</sup> It has been interpreted on the basis of the inaccessibility of the C<sub>60</sub> compact monolayer by charge-compensating electrolyte ions. In other words, only a small fraction of the surface-confined C<sub>60</sub> is electrochemically accessible and active.

The issue of accessibility and hence electrochemical activity is further manifested with a nanoparticle overlayer adsorbed onto

- (26) (a) Templeton, A. C.; Cliffler, D. E.; Murray, R. W. *J. Am. Chem. Soc.* **1999**, *121*, 7081. (b) Huang, T.; Murray, R. W. *Langmuir* **2002**, *18*, 7077.  
 (27) Luo, C.; Fujitsuka, M.; Watanabe, A.; Ito, O.; Gan, L.; Huang, Y.; Huang, C.-H. *J. Chem. Soc., Faraday Trans.* **1998**, *94*, 527.  
 (28) Chen, S.; Truax, L. A.; Summers, J. M. *Chem. Mater.* **2000**, *12*, 3864.  
 (29) Sauerbrey, G. Z. *Z. Phys. Chem.* **1959**, *155*, 206.  
 (30) (a) Chen, K.; Caldwell, W. B.; Mirkin, C. A. *J. Am. Chem. Soc.* **1993**, *115*, 1193. (b) Caldwell, W. B.; Chen, K.; Mirkin, C. A.; Babinec, S. *Langmuir* **1993**, *9*, 1945.  
 (31) Shih, S.-M.; Su, W.-F.; Lin, Y.-J.; Wu, C.-S.; Chen, C.-D. *Langmuir* **2002**, *18*, 3332.

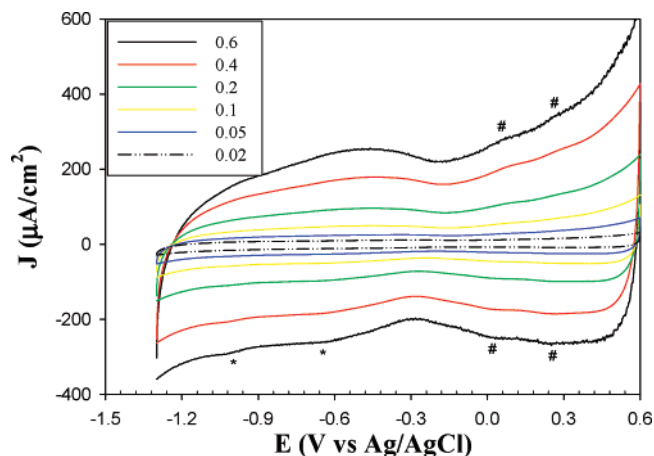


Figure 6. Cyclic voltammograms of an ATPAuC6 overlayer adsorbed onto a C<sub>60</sub>/cystamine self-assembled monolayer on gold (Figure 5) in a mixed solvent of toluene and acetonitrile (1/1 v:v) containing 0.1 M TBAP. Electrode area, 0.79 mm<sup>2</sup>. Potential scan rates shown as figure legends in V/s.

the C<sub>60</sub> surface. The corresponding voltammetric responses are shown in Figure 6. One can see that the C<sub>60</sub> voltammetric feature is even harder to identify, with two small peaks at  $-0.63$  and  $-1.02$  V (located by asterisks). Again, this can be accounted for by the inaccessibility of the C<sub>60</sub> molecules by electrolyte counterions upon redox reactions. However, the voltammetric responses from the particle overlayer are very similar to what we saw earlier with surface-immobilized nanoparticle assemblies,<sup>32</sup> with a series of quantized charging peaks (marked with #) within the potential range of 0 to +0.6 V. In the negative potential regime, the quantized charging peaks are almost invisible, most probably due to the interference of the C<sub>60</sub> faradaic reactions, as mentioned

above. In addition, a local current minimum can be found at  $\sim -0.24$  V, which is defined as the potential of zero charge (PZC) of the surface-adsorbed particle monolayer as observed previously.<sup>32</sup>

## CONCLUSION

Fullerene (C<sub>60</sub>) was tethered onto gold nanoparticle surfaces by amination reactions. These nanoscale composite materials exhibited unique spectroscopic and electrochemical properties. Significantly, it was observed that the quantum yield of the particle-bound C<sub>60</sub> was drastically larger than that of the pristine C<sub>60</sub>. Well-defined voltammetric responses were observed for both the C<sub>60</sub> faradaic reactions and nanoparticle quantized charging, whether the molecules were dissolved in solutions or immobilized onto the electrode surfaces. It is anticipated that the fabrication of organized surface assemblies of these nanocomposite materials might be exploited for optoelectronic applications.

## ACKNOWLEDGMENT

This work was supported, in part, by the National Science Foundation (CAREER Award CHE-0092760), the ACS Petroleum Research Fund, and the SIU Materials Technology Center. S.C. is a Cottrell Scholar of Research Corporation. Y.-S.S. thanks the Kentucky Space Grant Consortium, Kentucky Science and Engineering Foundation, and Western Kentucky University (Faculty Fellowship) for support.

## SUPPORTING INFORMATION AVAILABLE

TGA and FT-IR spectra of C<sub>60</sub>-ATPAuC6 nanoparticles. This material is available free of charge via the Internet at <http://pubs.acs.org>.

Received for review March 17, 2004. Accepted August 4, 2004.

AC0495891

(32) Chen, S. *J. Phys. Chem. B* **2000**, *104*, 663.